Formation of Water−in−Carbon Dioxide Microemulsions with a Cationic Surfactant: A Small−Angle Neutron Scattering Study

ARTICLE · NOVEMBER 2000

DOI: 10.1021/jp002202n

Formation of Water-in-Carbon Dioxide Microemulsions with a Cationic Surfactant: A Small-Angle Neutron Scattering Study

C. T. Lee, Jr.,[†] P. A. Psathas,[†] K. J. Ziegler,[†] K. P. Johnston,*[,†] H. J. Dai,[‡] H. D. Cochran,[‡,§] Y. B. Melnichenko,[||] and G. D. Wignall*[,||]

Department of Chemical Engineering, University of Texas at Austin, Austin, Texas 78712, Department of Chemical Engineering, University of Tennessee, Knoxville, Tennessee 37996, Chemical Technology Division, Oak Ridge National Laboratory, Oak Ridge, Tennessee 37831, and Solid State Division, Oak Ridge National Laboratory, Oak Ridge, Tennessee 37831

Received: June 16, 2000; In Final Form: September 8, 2000

The formation of water-in-carbon dioxide microemulsions with a cationic perfluoropolyether trimethylammonium acetate surfactant, PFPE−C(O)−NH−CH_2−$N^+(CH_3)_3$ CH_3COO^-, is reported over a range of temperatures (25−90 °C) and pressures (87.3−415 bar). Spherical droplets are observed by SANS with radii ranging from 16 to 36 Å for water-to-surfactant molar ratios (W_o) from 9.5 to 28. Porod analysis of the SANS data indicates an area of approximately 60 Å^2/surfactant molecule at the water−CO_2 interface, in reasonable agreement with the value of 72 Å^2 determined from the change in the droplet radius with W_o. The CO_2-phobic functionality between the surfactant headgroup and perfluoropolyether tail reduces CO_2 penetration of the tails, resulting in a smaller area/surfactant than in the case of an anionic perfluoropolyether surfactant [*Langmuir* **1997**, *13*, 3934]. A relatively rigid film, with a mean film rigidity ($2K + \bar{K}$) of approximately 1 k_BT, along with the strong partitioning of the surfactant toward CO_2 versus water, lead to the small, rigid, spherical water droplets in CO_2.

Introduction

Liquid or supercritical CO_2 (T_c = 31 °C, P_c = 73.8 bar) exhibits solvent properties which are tunable with pressure, and is essentially nontoxic and nonflammable. Dense CO_2 is nonpolar (unlike water) and has weak van der Waals forces (unlike oils). Water and CO_2 may be combined to form microemulsions as environmentally benign replacements for organic solvents to dissolve both polar and hydrophobic compounds. The existence of a bulk water domain in a water-in-CO_2 (W/C) microemulsion was demonstrated by several spectroscopic techniques with an ammonium carboxylate perfluoropolyether surfactant (PFPECOO$^-$$NH_4^+$).[1] Small-angle neutron scattering (SANS) experiments[2−4] on this and other systems confirmed the existence of microemulsions in the form of 20−35 Å spherical water droplets dispersed in CO_2, as supported by molecular simulations.[5] The area per surfactant in the microemulsion droplet, measured by SANS, is similar to that for the surfactant at the planar interface, as determined by tensiometry.[6,7] Dispersions of water in CO_2, whether on the nanometer (microemulsions)[1,4,6] or micrometer (emulsions)[8] scale, offer new possibilities for separations on the basis of polarity, and as media for reactions between polar and nonpolar molecules.[9,10]

To date, microemulsions in CO_2 have been formed only with a select few anionic surfactants. The formation of W/C microemulsions with cationic surfactants would offer additional opportunities in a variety of practical applications. Nucleophilic substitution,[9] catalytic hydrogenation,[10] and simple inorganic reactions,[11] as well as the formation of nanoparticles[12,13] have been performed in W/C systems stabilized with anionic ammonium carboxylate perfluoropolyether (PFPECOO$^-$ NH_4^+) surfactants. Since these nucleophilic substitution reactions involve the formation of a negatively charged transition state, the reaction rates may be expected to be higher in microemulsions formed with cationic surfactants, which are capable of stabilizing the transition state. Furthermore, in the reported case of catalytic hydrogenation in emulsions of water and CO_2,[10] an anionic, water-soluble catalyst was used. Again, the use of a cationic surfactant may be expected to increase the reaction rate, in this case by increasing the local concentration of the catalyst at the water−CO_2 interface where the reaction occurs.

It is often advantageous to use cationic surfactants to stabilize metal nanoparticles. For example, the formation of Pt nanoparticles by the reduction of platinum salts in the water pool of a water-in-oil (W/O) microemulsion occurred readily with cationic cetyltrimethylammonium bromide (CTAB), but not with anionic sodium octanoate, due to the low solubility of the platinum salts in the microemulsion.[14] Furthermore, quaternary ammonium salts have been shown to be capable of stabilizing noble-metal nanoparticles with negatively charged surfaces in organic solvents.[15]

Our objective is to extend the scope of W/C microemulsions to include a cationic surfactant and to characterize these microemulsions with phase behavior, SANS, and interfacial tension (IFT) measurements. Transitions from single-phase microemulsions to two-phase systems are described in terms of interdroplet interactions and changes in the natural curvature of the water−CO_2 interface on the basis of phase behavior and SANS data. The SANS data are modeled to determine the average droplet radius, polydispersity, and structure factor as a function of water-to-surfactant molar ratio (W_o), temperature,

* Authors to whom correspondence should be addressed.
[†] Department of Chemical Engineering, University of Texas at Austin.
[‡] Department of Chemical Engineering, University of Tennessee.
[§] Chemical Technology Division, Oak Ridge National Laboratory.
[||] Solid State Division, Oak Ridge National Laboratory.

10.1021/jp002202n CCC: $19.00
Published on Web 11/02/2000

and pressure. A linear fit of droplet radius versus the molar ratio of water to surfactant, corrected for the solubility of water in CO_2, is used to determine the surface area per surfactant molecule, which is compared to the value obtained from a Porod analysis of the data. The results are compared with previous studies of fluoroether anionic surfactants at water−CO_2 and water−perfluoropolyether oil interfaces. From the value of droplet radius and polydispersity determined from SANS, as well as interfacial tension measurements performed with surfactant at the water−CO_2 interface, a value of the mean film rigidity is calculated. The pH of the water core of the W/C microemulsions is determined from analysis of the UV−vis spectra of the hydrophilic indicator methyl orange.

Experimental Section

Materials. The surfactant of the form $F-(CF(CF_3)-CF_2-O)_n-CF(CF_3)-C(O)-NH-CH_2-N^+(CH_3)_3\ CH_3COO^-$ with a perfluoropolyether (PFPE) tail and a cationic trimethylammonium acetate (TMMA) headgroup was used in all experiments (abbreviated PFPE−TMAA). The surfactant had an average molecular weight of 1124 g/mol ($n = 4$) and was a gift from DuPont.[16] The surfactant was further purified to extract excess sodium acetate by successively stirring 5 g of the surfactant with 70 mL of water until the conductivity of the water phase was reduced from 600 μS/cm to less than 15 μS/cm. This corresponds to a remaining concentration of sodium acetate in the surfactant of approximately 0.5 mol %. Instrumen-grade CO_2 (Praxair) passed through an oxytrap (Oxyclear, model no. RGP-31-300) and Nanopure II water (Barnstead) were used as indicated. Deuterated water (99.9 atom %, Aldrich) was used in the SANS experiments. Methyl orange was purchased from Aldrich and used as received.

Microemulsion Phase Behavior. Microemulsions were prepared in a high-pressure, variable-volume view cell equipped with a sapphire window that permitted visual observation of microemulsion formation and phase behavior.[17] A piston inside the view cell was used to vary the pressure independently of temperature that remains constant within ±0.1 °C. System pressure was controlled with a syringe pump to within 1 bar by using CO_2 as the pressurizing fluid on the backside of the piston. The cell contents were mixed with a magnetic stir bar inside the cell. The microemulsion cloud point at each concentration was measured by decreasing the pressure from 450 bar until the clear, one-phase microemulsion became cloudy.

SANS Experiments and Analysis. The data were collected on the W. C. Koehler SANS facility[18] at the Oak Ridge National Laboratory with a 64 × 64 cm^2 area detector and element size ~1 cm^2. The neutron wavelength was $\lambda = 4.75$ Å ($\Delta\lambda/\lambda \sim 5\%$) and the beam at the sample was defined by an 8 mm cadmium iris. The sample−detector distance was 3.3 m and the data were corrected for instrumental backgrounds, detector efficiency, and the scattering from the cell windows for each detector element prior to radial averaging to give a Q-range of $0.010 < Q < 0.185$ Å^{-1}. The net intensities were converted to an absolute (±4%) differential cross section per unit sample volume (in units of cm^{-1}) by comparison with precalibrated secondary standards, based on the measurement of beam flux, vanadium incoherent cross section, the scattering from water, and other reference materials.[19] The coherent intensities of the sample were obtained by subtracting the (coherent) cross section of CO_2 (~10^{-2} cm^{-1}) and the (incoherent) cross section of the hydrogen atoms (~0.002 cm^{-1}) in the surfactant, and these formed only a minor correction to the sample data (<10%) except at higher Q. The variable-volume cell contained two, 5/8 in. diameter and 3/16 in. thick sapphire windows on opposite sides of the cell along the diameter,[20] resulting in a path length of 22.3 mm. The transmission through the samples was typically 70%, indicating that multiple scattering can be ignored.[21,22] System temperature was controlled to within ±0.2 °C with heating tape.

The SANS scattering intensity can be written as

$$I(Q) = \phi(\Delta\rho)^2 V_D P(Q,R) S'(Q,R,\phi) \quad (1)$$

where ϕ is the droplet volume fraction, $\Delta\rho$ is the scattering length density contrast, and V_D is the volume of a single droplet. The normalized form factor $P(Q,R)$, which is a function of the droplet size and shape, was calculated by assuming a Schultz distribution of polydisperse spheres with an average droplet radius of R^{avg} and a root-mean-square deviation in droplet sizes of $\sigma = R^{avg}/(Z+1)^{1/2}$ defined by the width parameter Z. This model of the form factor has been applied to both W/C[2,4] and W/O microemulsions,[23] and typically σ/R^{avg} is approximately 0.25. The structure factor, which depends on the interactions among droplets, was modeled by the modified Ornstein−Zernicke structure factor

$$S(Q,R,\phi) = 1 + \frac{S(0)}{1 + (Q\xi)^2} \quad (2)$$

where $S(0) = n_D k_B T k_T$, n_D is the droplet number density, k_T equals the osmotic isothermal compressibility, and ξ is the correlation length. The effect of droplet polydispersity on the structure factor was taken into account through the use of the modified structure factor $S'(Q) = 1 + \beta(Q)\,[S(Q) - 1]$, with $\beta(Q)$ given in Kotlarchyk and Chen.[23] Thus the model included five adjustable parameters, namely ϕ, R^{avg}, σ/R^{avg}, $S(0)$, and ξ. Although ϕ is, in principle, given by the known concentrations, it is advantageous to fit ϕ given the uncertainties in $\Delta\rho$ (see eq 1). In the Ornstein−Zernicke model, $S(0)$ is related to the isothermal osmotic compressibility and ξ is the correlation length; however, here they are just effective parameters. Note that cross-section Guinier analysis of the scattering data (a check for the linearity of $I(Q)Q^x$ versus Q^2) was consistent with spherical droplets ($x = 0$), as opposed to cylinders ($x = 1$) or lamella ($x = 2$) structures (not shown).[24]

The scattering length density difference was calculated by dividing the microemulsion into four regions, namely bulk D_2O, interfacial D_2O, surfactant tails, and solvent. In traditional W/O microemulsions, water with properties similar to that of bulk water exists for W_o greater than about 10. However, for W_o values less than about 10, the interfacial water is strongly associated with the surfactant headgroups.[25] As seen in Table 1, the scattering length densities of the bulk-water and interfacial-water regions of the microemulsion can be significantly different. The scattering length density of bulk water was calculated from the density of D_2O (1.107 g/cm^3), with the dissolved CO_2 taken into account.[26] The scattering length density of the interfacial-water region was calculated by assuming a total W_o of 10, and the surfactant headgroups were assumed to be located in this region. The scattering length density of the surfactant tails was calculated by assuming a surfactant bulk density of 1.8 g/cm^3.[27] Furthermore, solvent penetration into this tail region was accounted for by assuming that 10 CO_2 molecules solvate each surfactant tail.[2] The scattering length density of CO_2 was calculated from the bulk density of CO_2 at the given conditions accounting for the solubility of water in CO_2.[28] As seen in Table 1, the primary contrast is between the interfacial water and the surfactant tails, thus the reported droplet sizes are for the entire

TABLE 1: Calculated Scattering Length Densities ($\times 10^{-10}$ cm^{-2}) at 346 bar[a]

microemulsion domain	$T = 35$ °C	$T = 65$ °C	$T = 90$ °C
bulk D_2O	6.36	6.36	6.36
with dissolved CO_2[b]	6.35	6.35	6.35
interfacial D_2O[c]			
with surfactant head groups and CO_2	5.45	5.45	5.45
surfactant tails	3.85	3.85	3.85
with CO_2[d]	3.18	3.01	2.83
bulk CO_2	2.38	2.10	1.87
with dissolved D_2O [b]	2.42	2.19	2.01
$\Delta\rho$	2.27	2.44	2.62

[a] Assuming $\Delta V^{mix} = 0$ [b] CO_2−water mutual solubilities calculated from the Appendix. [c] Calculated for $W_o = 10$. [d] Calculated with 10 CO_2 molecules solvating each surfactant tail.

(bulk + interfacial) water region. Note that the regressed values of R^{avg}, σ/R^{avg}, $S(0)$, and ξ were insensitive to the value chosen for the scattering length density contrast, changing by only about 1% as $\Delta\rho$ was allowed to vary by as much as a factor of 2. Attempts to model the scattering data with a core and shell model for the form factor failed as the shell thickness always returned zero. This is likely the result of the diffuse nature of the bulk water-interfacial water and surfactant tail-bulk CO_2 boundaries.

Interfacial Tension Measurements. A modified version of a high-pressure pendant-drop tensiometer described previously[20,29] was used to measure the interfacial tension between deionized water and CO_2 ($\gamma_{W/C}$) at 90 °C and 346 bar. The apparatus consisted of a variable-volume view cell, an optical rail for proper alignment, a CCD video camera, and a computer. The view cell contained CO_2 and surfactant in the presence of excess water to ensure saturation of the CO_2 phase. Pendant drops of water were formed at the end of a stainless steel needle with blunt tip, with inside and outside diameter of 0.13 mm and 0.5 mm, respectively. The cell was thermostated within 0.1 °C. Several images were recorded as a function of time until the value of interfacial tension remained constant. Images of the entire contour of the drop were acquired with a Matrox Meteor II frame grabber and were analyzed by a software package from KSV (Finland) to solve the Laplace equation.

UV−Vis Absorption Measurements. The UV−vis spectra of the hydrophilic probe methyl orange was measured by flowing the contents of the phase behavior cell through a high-pressure spectroscopic cell with a gear pump (Baldor Electric Co.). The spectroscopic cell consisted of two optical grade sapphire windows forming a path length of 1.72 cm, as previously described.[30] Heating tape was used to control the temperature to within ±0.2 °C.

Results and Discussion

Microemulsion Phase Behavior. The results of the microemulsion phase behavior at 5.0 wt % (47 millimolal (m*m*)) and 2.5 wt % (23 m*m*) PFPE−TMAA in CO_2 are given as a function of W_o in Figures 1 and 2, respectively. The one-phase microemulsion region is above the curve in each plot. Two types of phase transitions were observed in this water/PFPE−TMMA/CO_2 system. The first type occurred upon lowering the pressure at constant temperature. At higher values of W_o, a second type of phase transition occurred as the temperature was lowered at constant pressure. Conductivity measurements performed on W/C microemulsions formed with a $PFPECOO^-NH_4^+$ surfactant have shown that the phase transition which occurs upon lowering the pressure is the result of attractive interactions between

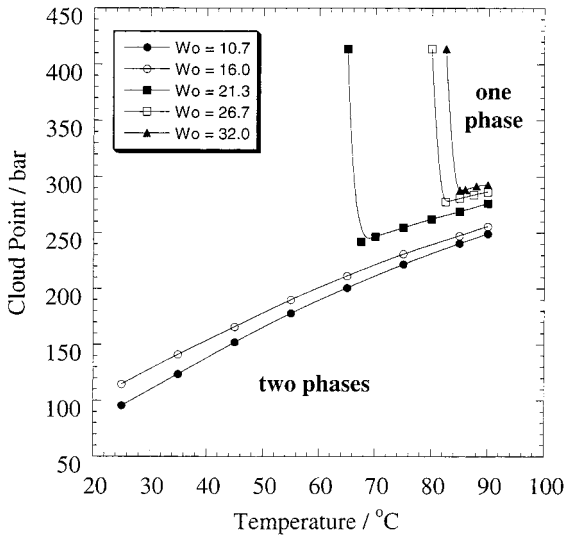

Figure 1. Phase behavior of the water/PFPE−TMMA/CO_2 system as a function of W_o at a surfactant concentration of 5.0 wt % (47 m*m*) in CO_2.

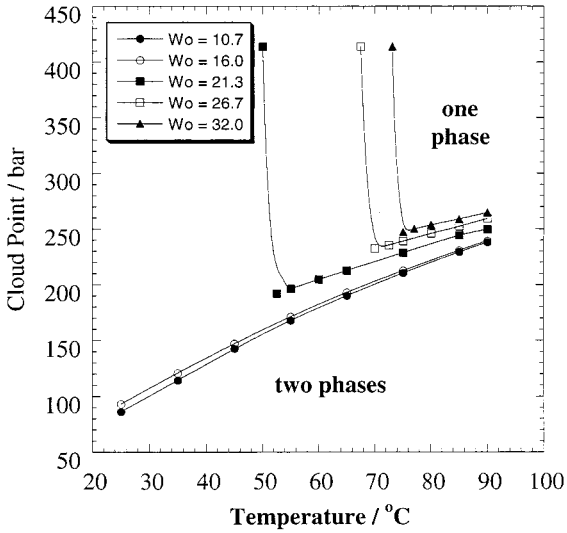

Figure 2. Phase behavior of the water/PFPE−TMMA/CO_2 system as a function of W_o at a surfactant concentration of 2.5 wt % (23 m*m*) in CO_2.

droplets, while the phase transition that occurs upon lowering the temperature is the result of the change in the natural curvature at the water−CO_2 interface.[17]

The phase transition due to droplet−droplet interactions results from a decrease in the density and, thus, solvent power, of CO_2 as the pressure is lowered at constant temperature. Decreasing the solvent power of CO_2 decreases solvent−tail interactions and thereby increases tail−tail interactions between neighboring microemulsion droplets. These tail−tail interactions eventually become strong enough to result in phase separation at the cloud point producing the formation of two microemulsion phases, one rich and one lean in droplet concentration (i.e., a critical-type transition).[31,32] Droplet−droplet interactions have been shown to increase with increasing droplet size.[33] Thus the phase separation resulting from droplet interactions occurs at higher densities (pressures) as W_o is increased, as seen in Figures 1 and 2. Furthermore, the phase separation occurs at higher densities as the surfactant concentration and, thus, droplet volume fraction, is increased. This is characteristic of a critical type transition for concentrations below the critical point.

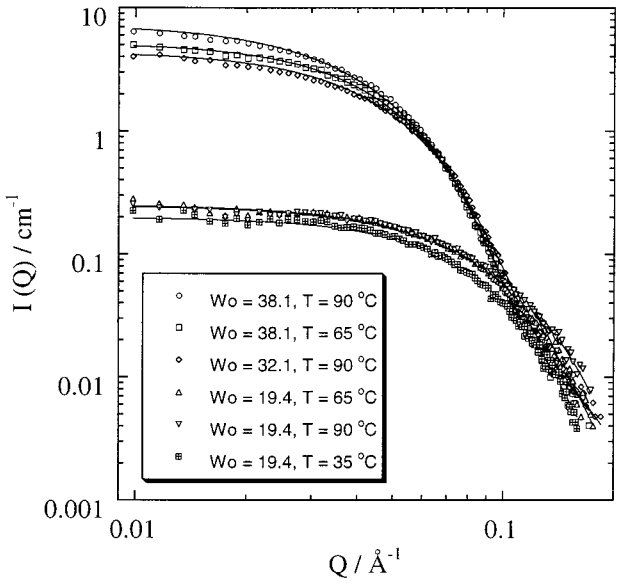

Figure 3. Scattering spectra versus W_o and T for W/C microemulsions at 5.0 wt % PFPE−TMMA in CO_2 and 346 bar, along with the fits obtained for a model with a form factor for a Schultz distribution of polydisperse spheres ($\sigma/R^{avg} = 0.25$) interacting via an Ornstein−Zernicke structure factor. Fitted model parameters are given in Table 2.

The phase transition resulting from a change in the curvature of the water−CO_2 interface results from a change in the relative solubilities of the surfactant in CO_2 and water. The surfactant is very soluble in CO_2 (at least 50 wt %)[17] and has a low solubility in water.[34] Thus, the natural curvature is about water. As the temperature is reduced at constant pressure, the density and correspondingly the solvent power of CO_2 increases, which increases the solubility of the surfactant in CO_2.[35] Furthermore, the solubility of anionic PFPE-based surfactants in water has been shown to decrease with decreasing temperature.[34] Thus, decreasing the temperature at constant pressure increases the relative affinity of the surfactant for CO_2, and, therefore, increases the natural curvature (decreases the natural radius) of the interface about water. Eventually, the natural curvature becomes less than the actual curvature, which is determined by W_o, resulting in phase separation as nearly pure water is expelled from the microemulsion phase. As W_o and thus droplet size is increased, the interface becomes less curved about water, hence the natural curvature-based phase separation occurs sooner, i.e., at higher temperatures, as W_o is increased, as seen in Figures 1 and 2. Note that the natural-curvature boundary occurs at lower temperatures as the surfactant concentration is decreased from 47 to 23 m*m* at a given W_o. This change results from an increase in the relative amounts of water dissolved in CO_2 compared to the droplet as the surfactant concentration is reduced, due to the relatively high solubility of water in CO_2 (to be discussed further below). This effectively lowers the corrected W_o value for the lower surfactant concentration, thereby increasing the actual curvature and suppressing the natural curvature phase separation.

Small-Angle Neutron Scattering. The SANS scattering curves for various W/C microemulsions formed with PFPE−TMMA along with the nonlinear least-squares model fits according to eqs 1 and 2 are shown in Figure 3. The accuracy of the fits of the model to the experimental scattering curves was ±5%, indicating that a Schultz distribution of polydisperse spheres with an Ornstein−Zernicke interaction is an accurate model for this system. The results of the model fits are given in pairs in Table 2 for the case when σ/R^{avg} is set equal to 0.25, as done previously,[2] and when it is a fitted parameter. Both approaches were employed because of the fact that the drop-contrast method applied here is not as accurate as shell-contrast[36] or contrast-variation[37] techniques in determining σ/R^{avg}. The values of W_o^{corr} were calculated by correcting for the solubility of (molecularly dissolved) D_2O in CO_2, assuming the CO_2 is saturated with water. A model of the binary water−CO_2 phase behavior used for this calculation is given in the Appendix.

The calculated values of droplet volume fraction ϕ^{calc} = (volume of dispersed D_2O)/(total volume) in Table 2 were determined assuming saturation of CO_2 with water as well as the bulk density of each component at a given T and P. In general, the fitted value of the droplet volume fractions agreed well with calculated values, further supporting the accuracy of the SANS model as well as the assumption of saturation of CO_2 with water. At $W_o^{corr} = 16.2$, the system was just barely into the two-phase region with an amount of excess phase slightly detectable by eye, while at $W_o^{corr} = 32.1$, the system was well into the two-phase region as evident from Figure 1. Thus it is not surprising that in both of these cases, ϕ^{fit} is significantly less than ϕ^{calc} calculated assuming a one-phase system.

In general, the fitted polydispersity σ/R^{avg} ranges from 0.22 to 0.32 with the exception of the results at a W_o^{corr} of 9.51. This polydispersity range is typical of both W/O[21,38] and W/C[2,4] microemulsions. However, for the lowest W_o^{corr} studied, the scattering data could be fit as either a polydisperse, noninteracting droplets, or as interacting droplets with relatively low polydispersity. In effect, the scattering curve responds to increased polydispersity and increased droplet interactions in an equivalent manner.[39] Eastoe et al. observed a similarly high value of polydispersity ($\sigma/R^{avg} = 0.40$) with a low value of $S(0)$ at the lowest W_o ($W_o \approx W_o^{corr} = 5$) in a W/C microemulsion

TABLE 2: SANS Fitted Parameters at 346 bar

W_o (W_o^{corr})	T (°C)	σ/R^{avg}	R^{avg} (Å)	ϕ^{fit}	$\phi^{calc\,a}$	$S(0)$	ξ (Å)	a_H (Å)
19.4 (9.51)	90	0.25	16.0	0.0044	0.0050	2.742	15.7[b]	60
		0.490	11.5	0.0079	0.0050	0.000[c]	*c*	
19.4 (13.6)	65	0.25	19.1	0.0063	0.0080	0.303	16.15	51
		0.293	18.1	0.0067	0.0080	0.107	7.781	
19.4 (16.2)	35[d]	0.25	20.2	0.0049	0.0110	0.511	13.11	*d*
		0.317	18.5	0.0043	0.0110	0.729	6.819	
32.1 (22.2)	90	0.25	31.6	0.0111	0.0116	0.992	8.975	60
		0.220	32.6	0.0126	0.0116	0.829	12.20	
38.1 (28.0)	90	0.25	35.9	0.0149	0.0143	1.048	14.71	62
		0.257	35.7	0.0147	0.0143	1.066	13.67	
38.1 (32.1)	65[d]	0.25	35.0	0.0151	0.0183	0.910	9.584	*d*
		0.248	35.0	0.0152	0.0183	0.927	10.22	

[a] Determined from the water loading minus the calculated solubility of water in CO_2. [b] This value was set to give a reasonable fit. [c] Fit returned $S(0) = 0$. [d] Two-phase system.

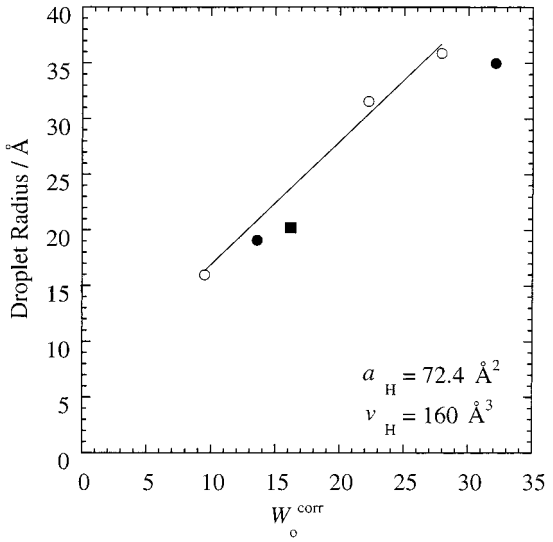

Figure 4. Linear fit of the droplet radius as a function of W_o^{corr} according to eq 4 at 90 °C and 346 bar (○). W_o^{corr} was calculated by assuming saturation of CO_2 with D_2O. For comparison, droplet radii at 35 and 65 °C (● and ■, respectively) are also included.

stabilized with the surfactant di-HCF4 and attributed it to relatively weak scattering.[4] Similarly, Kotlarchyk et al. reported that a "lack of statistical accuracy of the data" prevented a fit of σ/R^{avg} at the lowest W_o studied ($W_o = 8.2$) in the D_2O/AOT/decane microemulsion.[40] Conversely, Zielinski et al. assumed a fixed polydispersity of $\sigma/R^{avg} = 0.25$ and observed a relatively high value of $S(0)$ at the lowest W_o (calculated to be $W_o = 13.3$ and $W_o^{corr} = 9.9$) in a W/C microemulsion formed with $PFPECOO^-NH_4^+$. The magnitude of droplet interactions is expected to increase with increasing droplet size,[33] thus, the high-polydispersity case in Table 2 is more physically realistic. Furthermore, for small droplets the addition or removal of a surfactant or water molecule would result in a larger percentage change in drop size and correspondingly higher polydispersities at lower W_o values.[41]

A plot of the fitted average droplet radius versus the corrected value of W_o is shown in Figure 4. The data are linear as expected from the relation[21]

$$[1 + 2(\sigma/R^{avg})^2]R^{avg} = \left(\frac{3v_w}{a_H}\right)W_o^{corr} + \left(\frac{3v_H}{a_H}\right) \qquad (3)$$

where v_w is the molecular volume of water (D_2O), a_H is the area per surfactant molecule at the water−CO_2 interface, and v_H is the volume of the surfactant headgroup. From the slope of Figure 4, eq 3 gives an a_H of 72.4 Å^2 per surfactant molecule. Note that if the effect of polydispersity (i.e., the squared bracketed term in eq 3 is ignored, a value of 81.5 Å^2 is calculated. Furthermore, from the *y*-intercept of Figure 4, the volume of a surfactant headgroup is 160 Å^3, which corresponds to a radius of approximately 3.4 Å for a spherical headgroup. This number agrees well with the effective radius of the hydrated $(CH_3)_4N^+$ ion of 3.5 Å determined from partial molar volumes and molecular model calculations,[42] although this may be somewhat fortuitous given the limited number of data points applied to eq 3. Note that if the correction for the solubility of water in CO_2 is not made, the *y*-intercept in Figure 4 is less than zero, which is not physically realistic according to eq 3. Furthermore, errors in calculating the solubility of water in CO_2 would shift the data horizontally in Figure 4 by a constant value at a given *T* and *P*. This would change the fitted value of v_H but would not affect the value of a_H.

TABLE 3: Interfacial Tension Measurements and Film Rigidity Calculations at 90 °C and 346 bar

C_S (m*m*)	γ (mN/m)	$2K + \bar{K}^a$ (k_BT)	$2K + \bar{K}^b$ (k_BT)
0.334	0.52	0.99	0.98
0.445	0.55	1.05	0.98
0.667	0.49	0.93	0.98
0.889	0.49	0.93	0.98
1.33	0.50	0.95	0.98
1.78	0.51	0.97	0.98

[a] Calculated from eq 5. [b] Calculated from eq 6.

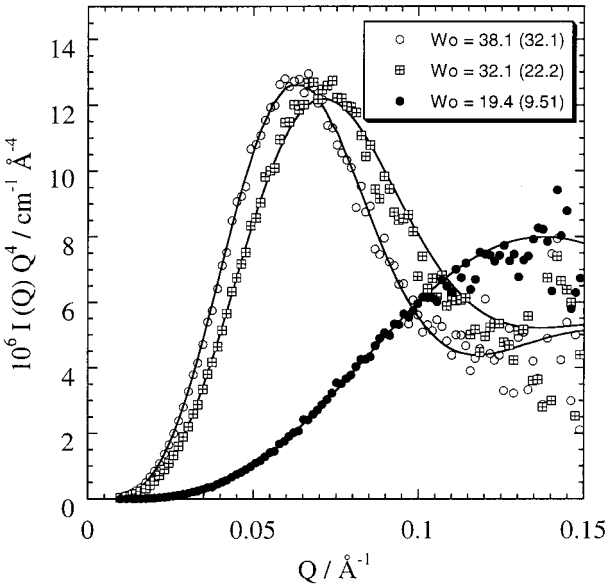

Figure 5. Porod analysis of the W/C microemulsions at 90 °C and 346 bar as a function of W_o. Values of W_o^{corr} are in parentheses.

The surface area per surfactant molecule can also be deduced from the SANS data with the model-independent Porod equation

$$[I(Q)Q^4]_{Q\to\infty} = 2\pi(\Delta\rho)^2\Sigma \qquad (4)$$

where Σ is the surface area per unit volume. Therefore, $a_H = \Sigma/N$, where *N* is the number of surfactant molecules at the water−CO_2 interface per unit volume. The IFT measurements (see Table 3) indicate that the critical microemulsion concentration (cμc) of PFPE−TMMA in CO_2 is less than 0.3 m*m* due to the constant value of the IFT over the concentration range studied. Thus, the majority of surfactant molecules reside at the interface and the total surfactant concentration (47 m*m*) can be used in eq 4. Porod plots at 90 °C are shown in Figure 5. As W_o and, thus, droplet size increases, the value of the first maximum and the first minimum, which appear at approximately $2.7/R$ and $4.5/R$ for monodisperse spheres, are shifted to larger *Q* as expected. Also, the first maximum for $W_o = 19.4$ is relatively broad, which is a characteristic of a polydisperse system. As is typical, the scattering data become less accurate at higher *Q*; however, a reasonable limiting value of $I(Q)Q^4$ is approximately 6×10^{-6} Å^{-4}cm^{-1}. This corresponds to an average a_H of 60 Å^2 at 90 °C as seen in Table 2, within approximately ±20 Å^2 due to the uncertainties in the limiting value of the Porod plot. This value agrees reasonably well with the value of 72.4 Å^2 obtained from a plot of droplet size versus W_o in Figure 4. Note that a_H decreased slightly with decreasing temperature as seen in Table 2, which has also been observed in IFT adsorption experiments at the water−CO_2 interface with $PFPECOO^-NH_4^+$. Therefore, only data at 90 °C were used to calculate a_H and v_H with eq 3 in Figure 4.

The values of the surface area per surfactant molecule seen in Figure 4 and Table 2 are at the lower end of the values previously obtained for surfactants in water−CO_2 systems. Specifically, a_H has been reported to be 107 Å^2 at $T = 65$ °C from IFT measurements[7] and can be estimated as 110 Å^2 from SANS data (determined from the reported droplet radius versus W_o at 35 °C in Zielinski et al.[2] using eq 3) with a PFPECOO$^-$-NH_4^+ surfactant, and reported as 87−98 Å with the di-HCF4 surfactant (a fluorinated analogue of AOT).[4] The results of a_H in Table 2 are intermediate between the values obtained in microemulsions stabilized with PFPECOO$^-$$NH_4^+$ in CO_2 and in a PFPE−oil (35−55 Å).[43]

The surface area per surfactant molecule is dependent on the interactions between neighboring hydrated surfactant headgroups and tails and solvent, as described theoretically.[7,44] Electrostatic repulsion is likely greater for the $-N(CH_3)_3^+$ headgroup of PFPE−TMMA compared to the $-COO^-$ headgroup of PFPE-$COO^-NH_4^+$ due to the relative inability of the counterion to closely approach the sterically hindered cationic headgroup.[45] This argument would incorrectly suggest a greater a_H in PFPE−TMMA versus PFPECOO$^-$$NH_4^+$ microemulsions, indicating that solvent−tail interactions are likely the cause of the lower a_H values obtained with PFPE−TMMA. The tails of the PFPE−TMMA surfactant contain an amide group between the PFPE tail and the cationic headgroup. CO_2 is not expected to solvate this amide group as effectively as the fluorocarbon portion of the surfactant tails. Therefore, CO_2 will mediate the attraction between neighboring surfactant tails less effectively as in purely fluorocarbon surfactants, resulting in a lower a_H. Furthermore, the amide group of the surfactant is capable of hydrogen bonding, which would tend to increase the attraction between neighboring tails and further lower a_H.

In brine/AOT/alkane systems, with equal amounts of water and oil, and where salt was added to cause the natural curvature to be about water, a_H was found to decrease as the oil molecular weight increased (less penetration), or as the magnitude of solvent−tail interactions decreased. It was concluded that a_H was determined by solvent−tail interactions rather that headgroup electrostatic repulsion, as concluded above for the water/PFPE−TMMA/CO_2 system.[44] A comparison of W/C and water-in-PFPE oil microemulsions with similar anionic PFPE surfactants further supports the concept that solvent penetration can influence a_H. The small CO_2 molecules penetrate the tails more effectively than the PFPE oil, contributing to an increase in a_H.[7]

As temperature is decreased at constant pressure, the solubility of water in CO_2 decreases, thus, W_o^{corr} increases for a given overall W_o. As seen in Table 2, W_o^{corr} increases from 9.51 to 13.6 as the temperature is decreased from 90 to 65 °C. However, the assumption that CO_2 is saturated with water needs to be justified since it is not obvious that the water in these small droplets has the same activity as a bulk water phase. The value of R^{avg}, measured by SANS, increases significantly with a decrease in temperature from 90 to 65 °C—from 16.0 to 19.1 or 11.5 to 18.1 Å, depending upon the choice of σ/R^{avg}. The regressed values of R^{avg} from the SANS data did not utilize the assumption concerning saturation of CO_2 by water or W_o^{corr}. Assuming that CO_2 is saturated with water, W_o^{corr} would be expected to increase from 9.51 to 13.6 over the same temperature range. Thus, the SANS data demonstrate that for W/C microemulsions with droplet concentrations where the total amount of water and the solubility of water in CO_2 are similar in value, the corrected value of W_o and, thus, the drop size can be tuned with temperature. The previous SANS studies on W/C microemulsions, which were performed by changing pressure at a constant temperature, exhibited only small (i.e., within experimental uncertainty) changes in droplet size due to a change in water partitioning between the droplet and CO_2.[2,4] This invariance results from the small change in solubility of water in CO_2 with pressure in the region of microemulsion formation, as seen in the Appendix. Note that this temperature tuning of drop size is unavailable in W/O microemulsions due to the relatively low solubility of water in alkanes compared to CO_2.

FT-IR experiments performed on D_2O-in-CO_2 microemulsions formed with PFPECOO$^-$NH4$^+$ at $W_o = 15$ have demonstrated that the bulk-D_2O peak decreased in intensity while the free-D_2O (i.e., D_2O that is soluble in CO_2) peak increased in intensity as temperature and, thus, the solubility of water in CO_2, was increased from 31 to 60 °C. The SANS data confirm this concept of tuning the drop radius at a given W_o by manipulating the water solubility in CO_2. In the FT-IR study, the interfacial-D_2O peak intensity remained constant as temperature was increased.[11] Therefore, it appears that the amount of water associated with the surfactant headgroups remains constant. The interaction between water and the ionic headgroups is strong; thus, it is unlikely that the interfacial water would partition into the CO_2 phase as temperature is increased. Furthermore, the water/PFPE−TMMA/CO_2 system in Table 2 with $W_o^{corr} = 9.51$ is near this interfacial water/bulk water cutoff. Therefore, the abnormally large polydispersity obtained in Table 2 at $W_o^{corr} = 9.51$ may result from an actual (i.e., non-Schultz distribution) polydispersity that is skewed to larger drop sizes because small drop sizes below $W_o = 10$ have a low probability of occurrence.

As seen in Table 2, the fitted values of $S(0)$ generally increase as W_o^{corr}, and the size of the water droplets, R^{avg}, increases from 13.6 to 22.2 and then to 28.0. This increase in $S(0)$ indicates that droplet interactions become stronger with increasing droplet size. As drop size increases, the volume of overlap between surfactant tails on neighboring droplets and, thus, the magnitude of tail−tail interactions are expected to increase.[33] Furthermore, the van der Waals attraction between the growing water cores will increase.[46] The result of increasing droplet interactions with droplet size has also been observed in W/C microemulsions formed with anionic surfactants.[2,4] The SANS data shed further light on the nature of the phase separation of the microemulsion. The relatively constant value of $S(0)$ as the temperature is lowered from 90 to 65 °C at $W_o = 38.1$ suggests that this phase transition is not due to interdroplet interactions. This suggestion is consistent with conductivity studies of the low-temperature phase transition boundary for PFPECOO$^-$$NH_4^+$ discussed above.

Rigidity of the Surfactant Film at the Water−CO_2 Interface. The interfacial tensions obtained at the water−CO_2 interface with the PFPE−TMMA surfactant are shown in Table 3. As seen in this Table, $\gamma_{w/c}$ reaches a limiting value of approximately 0.5 mN/m as the surfactant concentration is increased, indicating that the concentrations in Table 3 are above the cμc. The film rigidity, in the form of the sum $(2K + \bar{K})$, can be estimated from[47]

$$2K + \bar{K} = \gamma_{w/c} R_M^2 - \frac{k_B T}{4\pi} f(\phi) \qquad (5)$$

where K is the mean bending modulus, $\bar{K}$ is the Gaussian bending modulus, R_M is the maximum radius of the water core in the Winsor II (W/C microemulsion with excess water) system, and the function $f(\phi)$ arises from the entropy of mixing of the microemulsion droplets with volume fraction ϕ and can be

estimated as $f(\phi) \approx \ln(\phi) - 1$ for dilute systems. The mean film rigidity is also related to the droplet polydispersity by the equation[36]

$$2K + \bar{K} = \frac{k_B T}{8\pi(\sigma/R^{avg})^2} - \frac{k_B T}{4\pi} f(\phi) \qquad (6)$$

The values of interfacial rigidity calculated using eqs 5 and 6 are shown in Table 3. At 90 °C, the maximum droplet size can be estimated from R^{avg} determined from SANS at $W_o = 38.1$ (see Table 2). This estimation is based on the assumption that the system is near the natural-curvature (Winsor II) phase boundary as seen in Figure 1. The maximum radius of the water core R_M was estimated by subtracting the thickness of the surfactant headgroup determined from eq 3, i.e., 3.4 Å. The nominal value of $\sigma/R^{avg} = 0.25$ was used.

The values of $2K + \bar{K}$ obtained by the two equations are in excellent agreement, which lends credence to the polydispersity values obtained from the SANS analysis. The values of $2K + \bar{K} \geq k_B T$ indicate relatively rigid interfaces and are similar to values of $\sim 1\ k_B T$ obtained in water/AOT/octane[48] and water/DDAB/cyclohexane[49] microemulsions. Relatively small values of film rigidity ($< k_B T$) allow for greater fluctuations in the interfacial curvature and, thus, zero net curvature or bicontinuous structures.[50,51] Thus, the rigidities obtained in Table 3 are consistent with the droplet structure obtained from the SANS analysis. Film rigidities are expected to increase with either solvent penetration into the tail region, or an increase of ionic strength in the water cores. Because the solvent, CO_2, is a small, linear molecule, significant solvent penetration is likely. Indeed this was observed in the scattering length densities of the surfactant−tail region obtained in the SANS analysis above. Furthermore, CO_2 forms carbonic acid in water, which results in an ionic strength of 10^{-3} M in W/C microemulsion systems.[30,52] These two factors combined suggest that higher film rigidities are likely in W/C systems.

Microenvironment in the Microemulsion Droplets. The UV−vis spectra of the optical indicator methyl orange in W/C microemulsions formed with PFPE−TMMA at $W_o = 14$ at 35 and 90 °C are shown in Figure 6. The indicator partitions between the interfacial and bulk water regions of W/C microemulsions.[11] Thus, the spectra were deconvoluted yielding interfacial, as well as peaks of the indicator in the water core of the microemulsion. Spectra at a $W_o = 0$ were utilized to calibrate the interfacial peak, which changed with temperature from 407 nm (35 °C) to 395 nm (90 °C). Likewise, the absorption spectra of acidic and basic water solutions of methyl orange were taken to calibrate the location of the bulk water peaks (421, 464, 498, and 525 nm). The integrated extinction coefficients of the acid and base form of the indicator were determined over the appropriate wavelengths from solutions of methyl orange in water at pH 2 and pH 10. The microemulsion pH was calculated to be 3 ± 0.2 at 35 °C using the pK_a ($\sim$3.44) of the indicator,[53] assuming that the activity coefficients are unity, and using the ratio of basic to acidic concentrations, in agreement with values obtained in anionic W/C microemulsions.

From the deconvoluted spectra in Figure 6, the relative amount of the indicator at the interface as compared to the water core (shown as one peak) increases from 52% to 63% as the temperature is increased from 35 to 90 °C and W_o^{corr} decreases from 11.6 to 5.4. At $W_o^{corr} = 5.4$, the majority of the water in the microemulsion is expected to exist as interfacial water, thus, the relative amount of the indicator at the interface is larger. The above approach was used to analyze the spectra of a W/C microemulsion stabilized with the anionic $PFPECOO^-NH_4^+$ surfactant at $W_o^{corr} = 8$.[1] The relative amount of indicator at the interface is only 44% despite the fact that less bulk water is expected at $W_o^{corr} = 8$ compared to $W_o^{corr} = 11.6$. The anionic sulfonate group of the indicator is more strongly attracted to the interface for cationic versus anionic microemulsions as expected. This example illustrates that cationic W/C microemulsions may be expected to be advantageous for a number of reaction and materials formation processes involving negatively charged species, which are attracted to the interface.

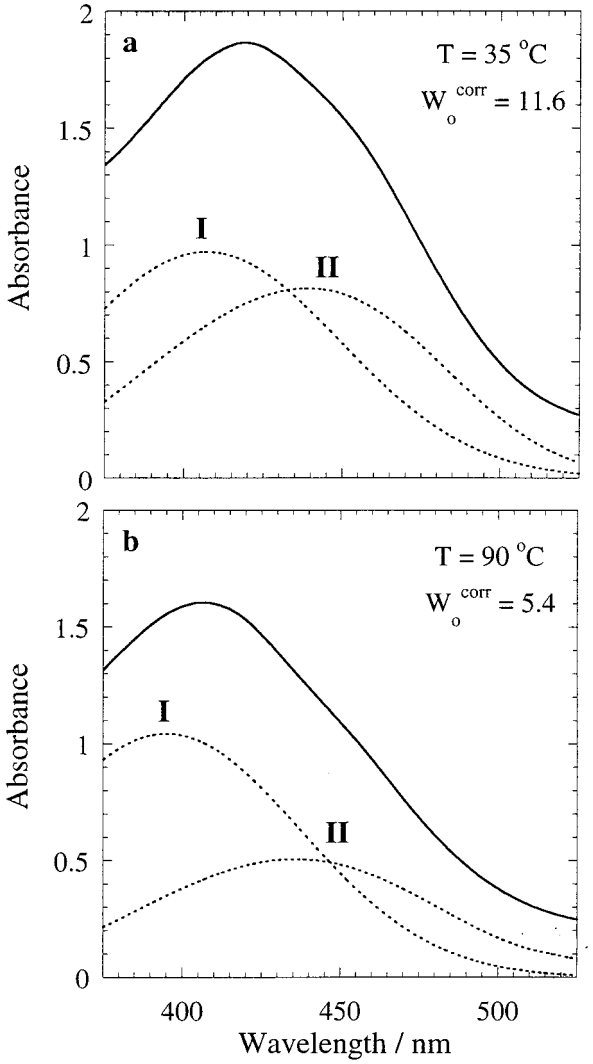

Figure 6. UV−vis spectra of the indicator methyl orange in W/C microemulsions stabilized with PFPE−TMMA at $W_o = 14$ and 346 bar for (a) $T = 35$ °C and (b) $T = 90$ °C. The spectra were deconvoluted into peaks of methyl orange at the interface (I), as well as peaks of methyl orange in bulk water(II).

Conclusions

Stable water-in-carbon dioxide microemulsions have been formed with a cationic perfluoropolyether surfactant to complement previous studies with anionic surfactants. The microemulsion is composed of rigid spherical droplets with radii ranging from 16 to 36 Å for water-to-surfactant molar ratios (W_o) ranging from 9.5 to 28. The interdroplet interactions are weak on the basis of the value of the structure factor at zero momentum vector, $S(0)$. These values for droplet radius and $S(0)$ are comparable to those observed for $PFPECOO^- NH_4^+$,[2] except

that the temperature is higher in the present study. The area per surfactant molecule determined by Porod analysis of the SANS data (60 Å^2) and by the change in the droplet radius with W_o (72 Å^2) are in reasonable agreement. The CO_2-phobic functionality between the headgroup and perfluoropolyether tail reduces CO_2 penetration of the tails, as reflected in a smaller area per surfactant molecule than in the case of $PFPECOO^-NH_4^+$. Measurements of interfacial tension at the CO_2−water interface along with droplet polydispersity, as determined by SANS, indicate a mean film rigidity ($2K + \bar{K}$) of approximately 1 k_BT. This relatively rigid film and the strong partitioning of the surfactant toward CO_2 relative to water lead to the small, rigid, spherical water droplets in CO_2. At low values of W_o, the droplet radius may be tuned with temperature at constant pressure in a one-phase microemulsion due to changes in the water solubility in CO_2. The pH of the water cores of the microemulsion is determined to be about 3 with the optical indicator methyl orange, in agreement with values obtained in W/C microemulsions stabilized with anionic surfactants. As expected, the anionic probe methyl orange is more strongly attracted to the interface for cationic relative to anionic W/C microemulsions. The ability to form cationic W/C microemulsions is of practical interest in a number of reaction and materials formation processes involving negatively charged species that are attracted to the interface.

Acknowledgment. We acknowledge support from DOE (DE-FG03-96ER14664), the Texas Advanced Technology Program, Welch Foundation, and the Separations Research Program at the University of Texas. Participants from Oak Ridge National Laboratory and the University of Tennessee were supported by the Divisions of Materials Sciences and Chemical Sciences of the DOE. The research at Oak Ridge supported by the U.S. Department of Energy under Contract DE-AC05-00OR22725 with the Oak Ridge National Laboratory, managed by UT-Battelle, LLC.

Appendix

To correct for the effect of the solubility of water in CO_2 on W_o and the amount of water dispersed (ϕ^{calc}), a phase behavior model was developed owning to the nonexistent experimental data at the temperatures of the SANS experiments (i.e., 90 °C). The values of W_o^{corr} and ϕ^{calc} were calculated by assuming that CO_2 was saturated with D_2O. Furthermore, the solubility of D_2O in CO_2 in the ternary (water/surfactant/CO_2) system was assumed equal to the solubility of water in CO_2 in the binary system due to the scarcity of CO_2−D_2O solubility data.[54] A phase behavior model was developed to calculate the solubility of water in CO_2 by equating the fugacity coefficient of each component in the CO_2-rich ("vapor") and water-rich ("liquid") phases. For water the equation is

$$(1 - x_c^{l})\phi_w^{sat}P_w^{sat}\exp\left(\frac{v_w^{avg}(P - P_w^{sat})}{RT}\right) = f_w^{l} = f_w^{v} = y_w^{v}\phi_w^{v}P \quad \text{(A1)}$$

where x_c^l and y_w^v are the mole fraction of CO_2 soluble in water and water soluble in CO_2, respectively, ϕ_w^{sat} is the fugacity coefficient of water at the saturation pressure P_w^{sat} and temperature T, v_w^{avg} is the average molar volume of water over the range of pressures from P_w^{sat} to the system pressure P, and ϕ_w^v is the fugacity coefficient of water in the vapor phase. The comparable equation for CO_2, based on the Krichevsky−Kasarnovsky equation which assumes an activity coefficient of unity and that $\bar{v}_{c,w} = \bar{v}_{c,w}^{\infty}$, which has been shown to be accurate for the water−CO_2 system for temperatures below 100 °C,[55] is given by

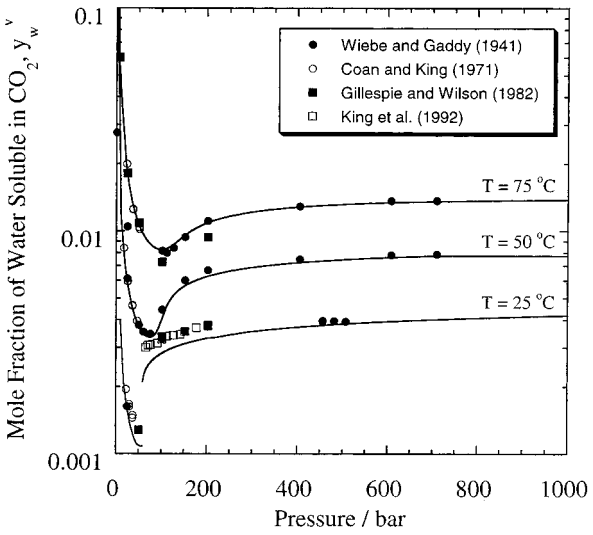

Figure A1. Comparison of experimental data of the solubility of water in CO_2 with fits of the phase behavior model described in the Appendix.

$$(1 - y_w^{v})\phi_c^{v}P = f_c^{v} = f_c^{l} = x_c^{l}H_{c,w}^{o}\exp\left(\frac{\bar{v}_{c,w}^{\infty}(P - P^{atm})}{RT}\right) \quad \text{(A2)}$$

where ϕ_c^v is the fugacity coefficient of CO_2 in the vapor phase, $H_{c,w}^o$ is the Henry's Law constant of CO_2 in water at atmospheric pressure P^{atm} and is taken from the correlation of Crovetta,[56] and $\bar{v}_{c,w}^{\infty}$ is the partial molar volume of CO_2 in water at infinite dilution and is approximately 32 cm^3/mol over the range of temperatures considered.[57] The fugacity coefficients ϕ_w^v and ϕ_c^v were calculated from the Stryjek and Vera improvement of the Peng−Robinson equation of state with Wong−Sandler mixing rules[58] coupled with the van Laar excess Gibbs energy model with regression parameters taken from Shyu et al.[59]

The comparison of the phase behavior model along with experimental data is given in Figure A1. The agreement with experimental data[28,60−62] is excellent, typically within 10%. The model predicts a discontinuity at 25 °C and 71.9 bar, which is in agreement with the experimental value of the triple point at 25 °C of 72.6 bar given by Kuenen and Robson.[63] The model accuracy for the solubility of CO_2 in water (not shown) was quite accurate as well, typically within 4%. With lack of experimental data at 90 °C and discrepancies in the experimental data at 100 °C,[64] this model is expected to give more accurate results at 90 °C than interpolation.

References and Notes

(1) Johnston, K. P.; Harrison, K. L.; Clarke, M. J.; Howdle, S. M.; Heitz, M. P.; Bright, F. V.; Carlier, C.; Randolph, T. W. *Science* **1996**, *271*, 624−626.

(2) Zielinski, R. G.; Kline, S. R.; Kaler, E. W.; Rosov, N. *Langmuir* **1997**, *13*, 3934−3937.

(3) Eastoe, J.; Bayazit, Z.; Martel, S.; Steytler, D. C.; Heenan, R. K. *Langmuir* **1996**, *12*, 1423−1224.

(4) Eastoe, J.; Cazalles, B. M. H.; Steytler, D. C.; Holmes, J. D.; Pitt, A. R.; Wear, T. J.; Heenan, R. K. *Langmuir* **1997**, *13*, 6980−6984.

(5) Salaniwal, S.; Cui, S. T.; Cummings, P. T.; Cochran, H. D. *Langmuir* **1999**, *15*, 5188−5192.

(6) Harrison, K.; Goveas, J.; Johnston, K. P.; O'Rear, E. A. *Langmuir* **1994**, *10*, 3536−3541.
(7) da Rocha, S. R. P.; Johnston, K. P. *Langmuir* **2000**, *16*, 3690−3695.
(8) Lee, C. T.; Psathas, P. A.; Johnston, K. P. *Langmuir* **1999**, *15*, 6781−6791.
(9) Jacobson, G. B.; Lee, C. T.; Johnston, K. P. *J. Org. Chem.* **1999**, *64*, 1201−1206.
(10) Jacobson, G. B.; Lee, C. T.; Johnston, K. P.; Tumas, W. *J. Am. Chem. Soc.* **1999**, *121*, 11902−11903.
(11) Clarke, M. J.; Harrison, K. L.; Johnston, K. P.; Howdle, S. M. *J. Am. Chem. Soc.* **1997**, *119*, 6399−6406.
(12) Ji, M.; Chen, X.; Wai, C. M.; Fulton, J. L. *J. Am. Chem. Soc.* **1999**, *121*, 2631−2632.
(13) Holmes, J. D.; Bhargava, P. A.; Korgel, B. A.; Johnston, K. P. *Langmuir* **1999**, *15*, 6613−6615.
(14) Boutonnet, M.; Kizling, J.; Stenius, P.; Maire, G. *Colloids Surf.* **1982**, *5*, 209−225.
(15) Bonnemann, H.; Brijoux, W.; Brinkman, R.; Fretzen, R.; Joussen, T.; Koppler, R.; Korall, B.; Neiteler, P.; Richter, J. *J. Mol. Catal.* **1994**, *86*, 129−177.
(16) Howell, J. L.; Hofmann, M. A.; Waterfeld, A.; Sipyagin, A. M.; Friesen, C. M.; Thrasher, J. S. In *216th ACS National Meeting*; Boston, MA, 1998; pp POLY 307.
(17) Lee, C. T.; Bhargava, P.; Johnston, K. P. *J. Phys. Chem. B* **2000**, *104*, 4448−4456.
(18) Koehler, W. C. *Physica* **1986**, *137B*, 320−329.
(19) Wignall, G. D.; Bates, F. S. *J. Appl. Crystallogr.* **1987**, *20*, 28−40.
(20) da Rocha, S. R. P.; Harrison, K. L.; Johnston, K. P. *Langmuir* **1999**, *15*, 419−428.
(21) Kotlarchyk, M.; Chen, S.-H.; Huang, J. S.; Kim, M. W. *Phys. Rev. A* **1984**, *29*, 2054−2069.
(22) Chen, S. H. *Annu. Rev. Phys. Chem.* **1986**, *37*, 351−399.
(23) Kotlarchyk, M.; Chen, S.-H. *J. Chem. Phys.* **1983**, *79*, 2461−2469.
(24) Glatter, O.; Strey, R.; Schubert, K.-V.; Kaler, E. W. *Ber. Bunsen-Ges. Phys. Chem.* **1996**, *100*, 323−335.
(25) Zulauf, M.; Eicke, H.-F. *J. Phys. Chem.* **1979**, *83*, 480−486.
(26) Wiebe, R.; Gaddy, V. L. *J. Am. Chem. Soc.* **1939**, *61*, 315−318.
(27) Chittofrati, A.; Boselli, V.; Visca, M.; Friberg, S. E. *J. Dispersion Sci. Technol.* **1994**, *15*, 711−726.
(28) Wiebe, R.; Gaddy, V. L. *Chem. Rev.* **1941**, *63*, 475−477.
(29) Harrison, K. L.; Johnston, K. P.; Sanchez, I. C. *Langmuir* **1996**, *12*, 2637−2644.
(30) Holmes, J. D.; Ziegler, K. J.; Audriani, M.; Lee, C. T.; Bhargava, P. A.; Steytler, D. C.; Johnston, K. P. *J. Phys. Chem. B* **1999**, *103*, 5703−5711.
(31) Kaler, E. W.; Billman, J. F.; Fulton, J. L.; Smith, R. D. *J. Phys. Chem.* **1991**, *95*, 458−462.
(32) Peck, D. G.; Johnston, K. P. *J. Phys. Chem.* **1991**, *95*, 9549−9556.
(33) Huang, J. S. *J. Chem. Phys.* **1985**, *82*, 480−484.
(34) Chittofrati, A.; Lenti, D.; Sanguineti, A.; Visca, M.; Gambi, C.; Senatra, D.; Zhen, Z. *Colloids Surf.* **1989**, *41*, 45−59.
(35) Heitz, M. P.; Carlier, C.; deGrazia, J.; Harrison, K.; Johnston, K. P.; Randolph, T. W.; Bright, F. V. *J. Phys. Chem. B* **1997**, *101*, 6707−6714.
(36) Gradzielski, M.; Langevin, D.; Farago, B. *Phys. Rev. E* **1996**, *53*, 3900−3919.
(37) Teubner, M. *J. Chem. Phys.* **1991**, *95*, 5072−5081.
(38) Eastoe, J.; Heenan, R. K. *J. Chem. Soc., Faraday Trans.* **1994**, *90*, 487−492.
(39) Azouz, I. B.; Ober, R.; Kakache, E.; Williams, C. E. *Colloids and Surfaces* **1992**, *69*, 87−97.
(40) Kotlarchyk, M.; Chen, S.-H.; Huang, J. S. *J. Phys. Chem.* **1982**, *86*, 3273−3276.
(41) Nicholson, J. D.; Clarke, J. H. R. In *Surfactants in Solution*; Mittal, K. L., Lindman, B., Eds.; Plenum Press: New York, 1984; Vol. 3; pp 1663−1674.
(42) Conway, B. E. *Ionic Hydration in Chemistry and Biophysics*; Elsevier: New York, 1981; Vol. 12.
(43) Baglioni, P.; Gambi, C. M. C.; Giordano, R.; Senatra, D. *J. Mol. Struct.* **1996**, *383*, 165−169.
(44) Aveyard, R.; Binks, B. P.; Fletcher, P. D. I. In *The Structure, Dynamics and Equilibrium Properties if Colloidal Systems*; Bloor, D. M., Wyn-Jones, E., Eds.; Kluwer Academic Publishers: Boston, 1990.
(45) Tanford, C. *The Hydrophobic Effect: Formation of Micelles and Biological Membranes*, 2nd ed.; Wiley-Interscience Publications: New York, 1980.
(46) Tingey, J. M.; Fulton, J. L.; Smith, R. D. *J. Phys. Chem.* **1990**, *94*, 1997−2004.
(47) Meunier, J.; Lee, L. T. *Langmuir* **1991**, *7*, 1855−1860.
(48) Kellay, H.; Meunier, J.; Binks, B. P. *Phys. Rev. Lett.* **1993**, *70*, 1485−1488.
(49) Eastoe, J.; Hetherington, K. J.; Dalton, J. S.; Sharpe, D.; Lu, J. R.; Heenan, R. K. *J. Colloid Interface Sci.* **1997**, *190*, 449−455.
(50) De Gennes, P. G.; Taupin, C. *J. Phys. Chem.* **1982**, *86*, 2294−2304.
(51) Kellay, H.; Binks, B. P.; Hendrikx, Y.; Lee, L. T.; Meunier, J. *Adv. Colloid Interface Sci.* **1994**, *49*, 85−112.
(52) Niemeyer, E. D.; Bright, F. V. *J. Phys. Chem. B* **1998**, *102*, 1474−1478.
(53) Hone, D. C.; Robinson, B. H.; Steytler, D. C.; Glyde, R. W.; Galsworthy, J. R. *Langmuir* **2000**, *16*, 340−346.
(54) Wilhelm, E.; Battino, R.; Wilcock, R. J. *Chem. Rev.* **1977**, *77*, 219−262.
(55) Carroll, J. J.; Mather, A. E. *J. Solution Chem.* **1992**, *21*, 607−621.
(56) Crovetto, R. *J. Phys. Chem. Ref. Data* **1991**, *20*, 575−589.
(57) Dhima, A.; Hemptinne, J.-C. d.; Jose, J. *Ind. Eng. Chem. Res.* **1999**, *38*, 3144−3161.
(58) Wong, D. S. H.; Sandler, S. I. *AIChE J.* **1992**, *38*, 671−679.
(59) Shyu, G.-S.; Hanif, N. S. M.; Hall, K. R.; Eubank, P. T. *Fluid Phase Equilib.* **1997**, *130*, 73−85.
(60) Coan, C. R.; King, A. D., Jr. *J. Am. Chem. Soc.* **1971**, *93*, 1857−1862.
(61) Gillespie, P. C.; Wilson, G. M. *Vapor−Liquid and Liquid−Liquid Equilibria: Water−Methane, Water−Carbon Dioxide, Water−Hydrogen Sulfide, Water−n-Pentane, Water−Methane−n-Pentane*; GPA Research Report RR-48, 1982.
(62) King, M. B.; Mubarak, A.; Kim, J. D.; Bott, T. R. *J. Supercrit. Fluids* **1992**, *5*, 296−302.
(63) Kuenen, J. P.; Robson, W. G. *Philos. Mag.* **1899**, *48*, 180−203.
(64) Mather, A. E.; Franck, E. U. *J. Phys. Chem.* **1992**, *96*, 6−8.